Available online at www.sciencedirect.com
ScienceDirect
Trans. Nonferrous Met. Soc. China 32(2022) 709−720
Transactions of Nonferrous Metals Society of China
www.tnmsc.cn

Interaction mechanism between arsenate and fayalite-type copper slag at high temperatures

Da-wei WANG[1], Zong-wen ZHAO[1], Zhang LIN[1,2], Yan-jie LIANG[1,2], Li KANG[1], Bing PENG[1]

1. School of Metallurgy and Environment, Central South University, Changsha 410083, China;
2. Chinese National Engineering Research Center for Control & Treatment of Heavy Metal Pollution, Changsha 410083, China

Received 26 January 2021; accepted 7 December 2021

Abstract: The interaction mechanism between sodium arsenate and fayalite-type copper slag at 1200 °C was investigated through XRD, XPS, HRTEM, TCLP and other technical means and methods. The results indicated that the proportions of sodium arsenate in the slag and flue gas phases were approximately 30% and 70%, respectively. The addition of sodium arsenate depolymerized the fayalite structure and changed it from a crystalline state to an amorphous state. The fayalite structural changes indicated that the [AsO_4] tetrahedron in sodium arsenate combined with the [SiO_4] tetrahedron and [FeO_4] tetrahedron through bridging oxygen to form a silicate glass structure. The TCLP test results of the samples before and after the high temperature reaction of fayalite and sodium arsenate showed that after high temperature reaction, fayalite could effectively reduce the leaching toxicity of sodium arsenate, reducing the leaching concentration of arsenic from 3025.52 to 12.8 mg /L before and after reaction, respectively.

Key words: fayalite; sodium arsenate; depolymerization reaction; silicate glass structure

1 Introduction

Copper smelting is the most important and complex source of arsenic pollution [1−3]. During the copper pyrometallurgical process, the majority of arsenic is volatilized and moved into SO_2 flue gas as As_2O_3 and then transformed into arsenic-containing waste acid by washing with dilute acid in the flue gas cleaning system [4]. In the slagging process, approximately 22 wt.% arsenic enters into the copper smelting slag [5]. It is estimated that approximately 24.6 million tons of copper smelting slag is discharged into the environment around the world per annum. LIU and YIN [6] determined that this byproduct should be classified as a hazardous material due to the presence of arsenic. In addition, landfill disposal of such arsenic-containing copper slag not only consumes land resources but also increases potential environmental pollution with the slow release of arsenic. Therefore, it is important to find effective ways to manage this kind of copper slag.

Past researches primarily focused on the presence of arsenic in minerals. LI et al [7] adopted synchrotron X-ray absorption spectroscopy and single-crystal electron paramagnetic resonance to study the arsenic speciation in $CaB_2Si_2O_8$ and determined that arsenic was present in both the +3 and +5 oxidation states and preferentially occupied the Si site. FILATOV et al [8] found that tetrahedral AsO_4 and SiO_4 shared a common oxygen atom in the $K[(Al,Zn)_2(As,Si)_2O_8]$ crystal, namely, the substitutions of elevated amounts of Si^{4+} ions by As^{5+} ions in silicates. PAPE et al [9] found that arsenic was added to pyrite during crystallization at

Corresponding author: Yan-jie LIANG, Tel: +86-13667353405, E-mail: LiangyanjieCSU@163.com
DOI: 10.1016/S1003-6326(22)65827-8
1003-6326/© 2022 The Nonferrous Metals Society of China. Published by Elsevier Ltd & Science Press

ambient temperature, and the main arsenic dissolution mechanism replaced the octahedral Fe^{2+} ions sites and tetrahedral S^{-} ions sites with arsenic. The main mineral phase in the copper slag is Fe_2SiO_4 [10,11], which has a similar structure to pyrite where silicon (Si) atoms are tetrahedral sites with isolated tetrahedra [SiO_4] units, and iron (Fe) atoms are octahedral sites surrounded by six oxygen atoms [12]. Arsenic dissolution in the fayalite-based copper slag is similar to that of pyrite.

Although some researches have been conducted on arsenic in nonferrous metallurgical slag, there are many unanswered questions on how to prevent arsenic pollution. It is important to understand the interaction between arsenic and copper slag to control arsenic pollution since arsenic in copper slag limits its use. In copper production, a considerable part of arsenate is produced from smelting electric collection dust when the gaseous arsenic oxide is oxidized [13]. To control arsenic pollution and recover metals, the high arsenic content from smelting electric collection dust is recirculated during the smelting process [5,13]. REDDY and FONT [14] determined that arsenate was the most stable arsenic species in copper smelting at high temperatures up to 1573 K, which indicated that arsenic entered the slag phase in the form of arsenate. In addition, ZHAO et al [15] found that arsenate formed chemical bonds with SiO_4 tetrahedra by bridging oxygen in the silicate-based glass. This research provides an important clue that the arsenic dissolution mechanism in fayalite-based copper slag is linked to the interaction between arsenate and fayalite. This hypothesis requires experimental verification.

The interaction mechanism of arsenate and copper slag at high temperature is of great significance for revealing the existence state of arsenic in copper slag and controlling the pollution of arsenic in copper slag. However, there are few reports in this area of research. In this work, typical arsenate (sodium arsenate) and synthesized fayalite were used to study the dissolution mechanism of arsenic in fayalite-based copper slag. In addition, a joint characterization method was used to characterize the reaction process and reveal possible fayalite structure changes caused by arsenic dissolution.

2 Experimental

2.1 Materials

Sodium arsenate (Na_3AsO_4) was obtained from $Na_3AsO_4·12H_2O$ (supplied by Sinopharm Chemical Reagent Co., Ltd.) dehydrated at 700 °C. High purity argon gas (99.999 vol.%) was used as the protective atmosphere. Synthetic fayalite (Fe_2SiO_4) was obtained as described in previous study [11]. The XRD pattern shown in Fig. 1 indicated that Fe_2SiO_4 was the main mineral phase in the final product.

2.2 Experimental procedures

The experiments were carried out in a portable controlled atmosphere furnace (OTF−1200X, Hefei Kejing Materials Technology Co., Ltd.) (Fig. 2). The temperature was controlled within ±1 °C using a B-type thermocouple and a proportional integral differential controller. Different amounts of Na_3AsO_4/

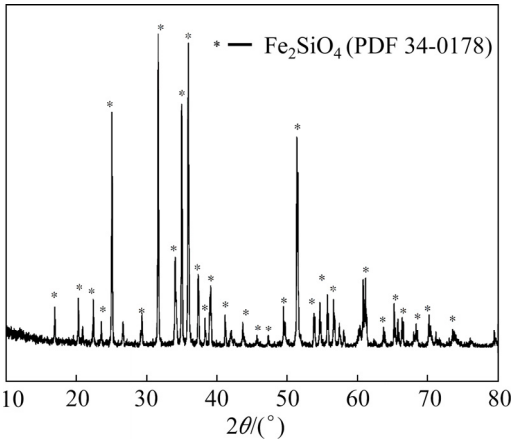

Fig. 1 XRD pattern of synthetic fayalite (Fe_2SiO_4)

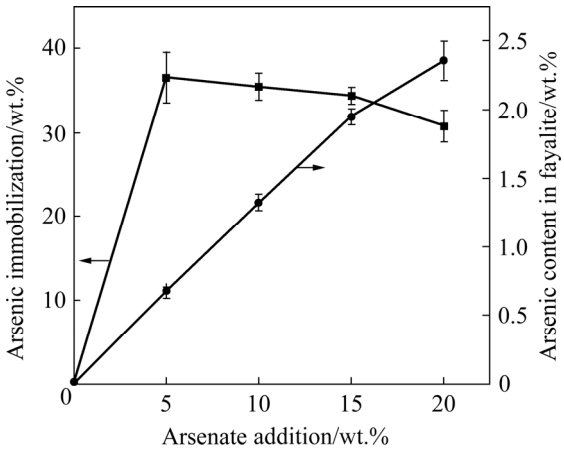

Fig. 2 Arsenic distribution ratio and mass fraction in fayalite slag with different initial arsenate additions

Na_2CO_3 were added to the fayalite to study the dissolution behavior of arsenate in the fayalite, with the specimen compositions listed in Table 1. The Sample S1 in Table 1 is a blank control sample with only fayalite added; Samples S2 to S5 are gradually added with sodium arsenate, increasing its content from 5 to 20 wt.%. Since arsenic is added to the sample in the form of sodium arsenate, to detect the influence of sodium ions on the structure of fayalite, a control Sample S6 is specially set up. The specimens were prepared by firstly blending a mixture of Na_3AsO_4 and Fe_2SiO_4 evenly via grinding in an agate mortar. Then, the mixture was pressurized in a mounting press with 50 MPa. Subsequently, the cylindrical-shaped mixed material was placed into a corundum crucible (inner diameter of 30 mm, outer diameter of 35 mm and height of 37 mm). Afterward, the specimens were heated at 1200 °C for 60 min. To keep the reaction under an inert atmosphere, high purity argon gas was continuously supplied into the furnace with a flow of 100 mL/min as measured by a flow meter. After the reaction, the melts were quenched to room temperature.

2.3 Analytical methods

The specimen phase compositions and structural properties were investigated by X-ray diffraction (XRD, D/max2550 VB + 18 kW) with steps of 10 (°)/min and 2θ ranging from 10° to 80°. Fourier transforms infrared (FTIR) spectra were collected in the range of 400−2000 cm^{-1} using a Nicolet IS10 spectrometer at 4 cm^{-1} resolutions. Magnetic properties were measured using a physical property measurement system (PPMS DynaCool, Quantum Design, USA) at room temperature. XPS was performed with a Thermo Scientific ESCALAB 250Xi using an Al K_α X-ray source (1486.6 eV). To compensate for the charging effects, all of the spectra were calibrated with graphitic carbon, with a binding energy of 284.8 eV, as a reference. Mossbauer spectra were obtained at room temperature with an effective thickness of 10 mg/cm^2 Fe in the conventional time mode with a Mossbauer spectrometer (Wissel, GER) in the transmission geometry using a 57 Co/Pd source. High-resolution transmission electron microscopy (HRTEM) was performed by an FEI Tecnai G2 F20 S T-WIN in two institutions. The TCLP test method standard comes from USEPA method 1311.

3 Results and discussion

3.1 Arsenate content distribution at high temperature

Sodium arsenate was set as the dominant arsenic phase in copper slag because the arsenate volatilization rate at high temperatures is lower, and the arsenic dissolution process was observed in our experiment. Additionally, arsenate is a common arsenic phase in raw and return materials, such as smelting ash. Figure 2 shows the fayalite slag distribution ratio and mass fraction with different initial arsenate additions. The results showed that with increasing arsenate dosage in raw materials, the arsenic mass fraction in fayalite slag increased significantly, but the arsenic distribution proportion in slag decreased. The mass fraction of arsenic in slag increased from 0.67% (S2) to 2.35%, and the arsenic distribution ratio decreased from 34 to 30 wt.%. This finding suggested that the proportion of arsenic resolved in the slag was approximately 30 wt.%, while most of the arsenic (approximately 70 wt.%) entered the flue gas. This distribution ratio agreed with other reports [16−18].

3.2 Arsenate and fayalite slag phase transformation

Fayalite is a mineral with a simple phase composition and weak magnetism. The reaction of

Table 1 Raw material mass and experiment reaction condition

Sample	m(Fayalite)/g	m(Na_3AsO_4)/g	m(Na_2O)/g	Temperature/°C	Time/min	Arsenate content/wt.%
S1	30	0	0	1200	60	0
S2	28.5	1.5	0	1200	60	5
S3	27.0	3.0	0	1200	60	10
S4	25.5	4.5	0	1200	60	15
S5	24.0	6.0	0	1200	60	20
S6	27.31	0	2.69	1200	60	0

arsenate and fayalite at 1200 °C can induce phase and magnetism changes. Therefore, we used XRD, hysteresis loop tests and HRTEM to study these changes.

Figure 3(a) shows the XRD results for the specimens with initial arsenate contents varying from 0 to 20 wt.%. The only crystalline phase identified in S1 was Fe_2SiO_4. With increasing arsenic content, the fayalite peak intensities presented a weakening tendency (from S1 to S3) and eventually disappeared at S4−S5. This phenomenon proved that introducing arsenate gradually decomposed the fayalite phase to Fe_3O_4, which was formed from the oxidation of Fe^{2+} ions in fayalite by As^{5+} ions in Na_3AsO_4. Simultaneously, the cold end of the quartz tube was covered by a metallic sheen layer (Fig. 3(c)) in the experiment, which resulted from metal arsenic steam condensation produced as in Eq. (1). Interestingly, XRD has not detected silicon-containing or arsenic-containing compounds, which suggested the amorphous form of these substances [19]. We note that by controlling the Na_2CO_3 content, the Na^+ ions in S6 were guaranteed to be equal to those in S5. The XRD pattern of S6 (Fig. 3(b)) was used to illustrate the effect of Na^+ ions derived from Na_3AsO_4 on the fayalite. The only crystal phase identified in S6 was FeO, which indicated that the fayalite structure was depolymerized. Na^+ ions could break the Si—O—Fe/Fe—O—Fe bond in fayalite and release FeO. Importantly, we observed a small hump at approximately 2θ=35°, which is a typical characteristic of the amorphous state [20]. This result provides evidence of the silicate amorphous transformation caused by Na^+ ions.

$$AsO_4^{3-}+Fe^{2+}\rightarrow As+Fe^{3+} \quad (1)$$

$$Fe^{2+}+Fe^{3+}+O^{2-}\rightarrow Fe_3O_4 \quad (2)$$

$$Na_2O+2FeO\cdot SiO_2(\text{crystal})\rightarrow 2FeO+Na_2O\cdot SiO_2\ (\text{amorphous}) \quad (3)$$

The measured magnetic properties of specimens with different arsenate contents are depicted in Fig. 4(a), and the saturation magnetization of samples at 1600 kA/m is shown in Fig. 4(b). The results showed that with increasing arsenate addition, there was an increasing trend in

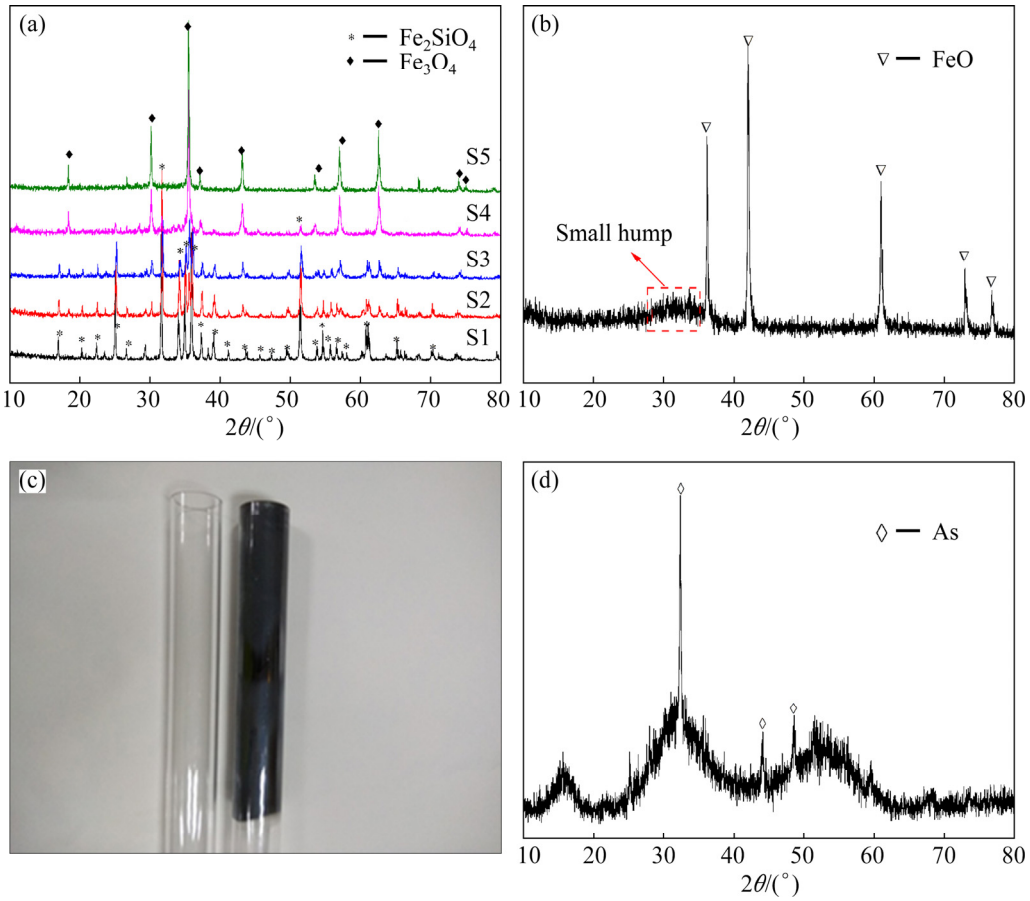

Fig. 3 XRD patterns of specimens with different initial arsenate additions (a) and with Na_2O (b), picture of quartz tube (c), and XRD pattern of metal arsenic (d)

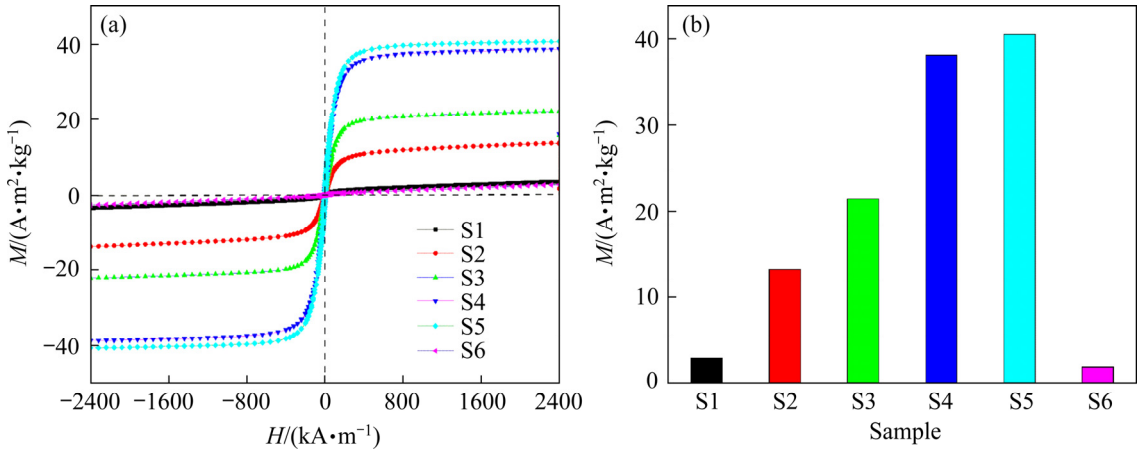

Fig. 4 Magnetic hysteresis loops (a) and magnetization in 1600 kA/m (b) of specimens with different arsenate additions and with Na_2O

fayalite specimen saturation and remanent magnetization. The specimen without arsenate (S1) had a room temperature saturation magnetization of 3.45 A·m^2/kg. It is known that fayalite is an orthorhombic system with two metal portions of Fe^{2+} and Fe^{3+} ions in the structure [21]. Fe^{2+} and Fe^{3+} ions are connected by the nonmagnetic oxygen ion [—O—], and the magnetic moment is antiparallel; therefore, S1 exhibited weak magnetism. After adding more arsenate, the saturation magnetization increased from 13.65 (S2) to 41.23 A·m^2/kg (S5). The significant increase in saturation magnetization could be attributed to the formation of Fe^{2+} ions oxidized by As^{5+} ions and the formation of Fe—O—Fe transition state bonds in Fe_3O_4. More gaps appeared in the fayalite structure due to the smaller Fe^{3+} ionic radii [22]. Owing to the overlapping and inner layer with unfilled electrons on the oxygen site, the unpaired electrons may superexchange with neighboring 3d orbital Fe^{2+} electrons, leading to incomplete reverse magnetic moment neutralization and ferromagnetic properties. Therefore, the magnetic properties of the whole structure were significantly enhanced. The S6 saturation magnetization was the lowest because Na^+ ions destroyed the fayalite structure and released FeO. FeO has antiferromagnetic properties [23] and showed small saturation magnetization in the test.

HRTEM experiments were performed to detect the effect of arsenic on the internal slag structure, and the results are presented in Fig. 5. There were obvious lattice fringes in S1, which is a typical characteristic of highly crystallized substances. According to the XRD results, it was reasonable to assign these lattice fringes to fayalite. However, the lattice fringes were gradually replaced by disordered speckles with increasing arsenic (Figs. 5(b) and (c)). SONG et al [24] assigned this kind of disordered speckle to amorphous substances. Based on a previous study [15], it was reasonable to believe that the amorphous substances were due to the matrix with [AsO_4] tetrahedrons, [SiO_4] tetrahedrons, and [FeO_4] tetrahedrons. These results indicated that adding arsenate depolymerized the fayalite structure and changed it from a crystalline state to an amorphous state. Specifically, the isolated crystal [SiO_4] tetrahedron derived from fayalite transformed into an amorphous [SiO_4] tetrahedron.

3.3 Fayalite structure evolution

We performed a spectroscopic analysis of the reaction products, including FTIR, XPS and Mossbauer, to further characterize the reaction between arsenic and fayalite. We found that the fayalite structure depolymerized and released [SiO4] and [FeO4] tetrahedra with increasing arsenate content. Subsequently, the [AsO_4] tetrahedrons in arsenate combined with the [SiO_4] and [FeO_4] tetrahedrons by bridging oxygen to form a glass network structure, which was the key mechanism for arsenic dissolution in fayalite.

The FTIR results for the specimens are shown in Fig. 6(a). Table 2 lists the main FTIR absorption peaks and associated groups [25−28]. These results show that with increasing arsenate content, the fayalite structure was gradually depolymerized.

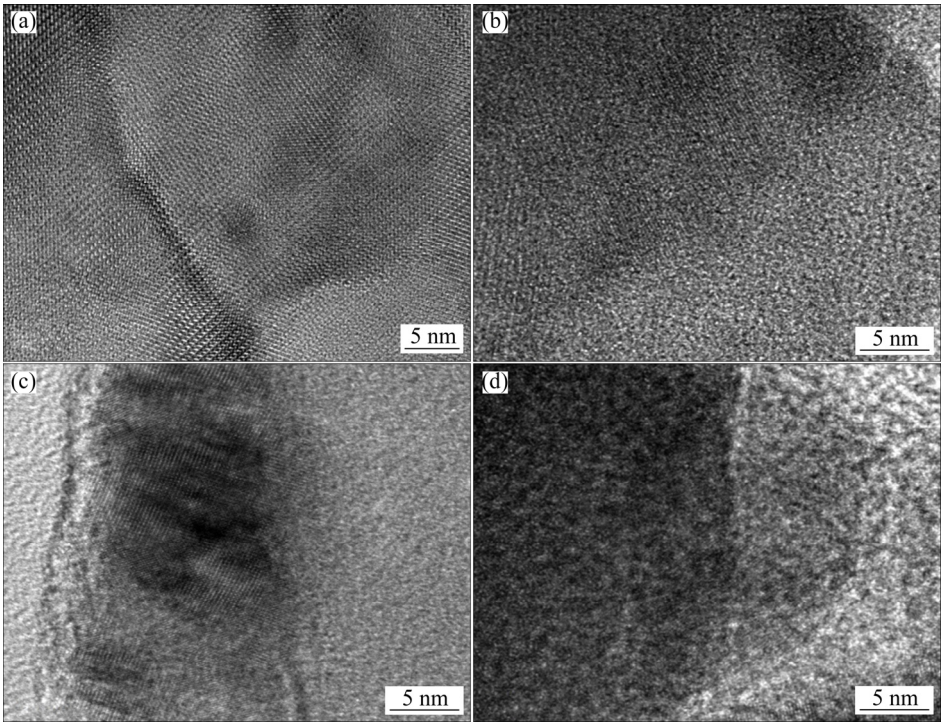

Fig. 5 HRTEM images of specimens with different initial arsenate additions: (a) S1; (b) S3; (c) S5; (d) S6

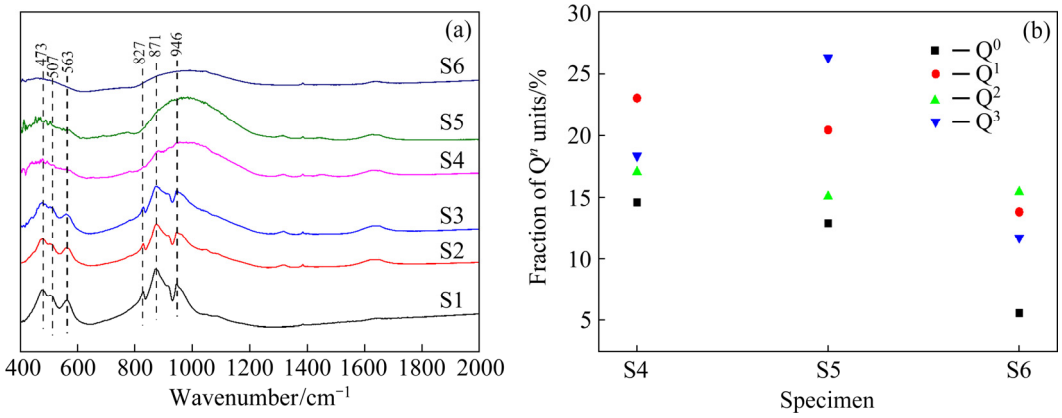

Fig. 6 FTIR spectra of specimens with different initial arsenate additions and with Na_2O (a), and fraction of Q^n units with different initial arsenate additions and with Na_2O (b)

Table 2 Assignments of different vibrational bands from FTIR spectra

Wavenumber/ cm^{-1}	Assignment
473	Si—O—Si bending vibration (Q^4)
507	SiO_4 related vibration
563	SiO_4 bending model
827, 871, 946	Characteristic peaks for fayalite crystals
750−1160	Si—O stretching vibration

Subsequently, we observed an amorphous transformation, which indicated the increased degree of polymerization (DOP) in the specimen. Figure 6(a) shows the characteristic peaks of fayalite crystals, including the peaks at approximately 946, 871, and 827 cm^{-1}, which became weak (S2, S3) and even disappeared (S4, S5). This change proved fayalite crystals depolymerized due to the increasing arsenate content. In addition, a new broad peak appeared near 800−1200 cm^{-1} in S4 and S5, which is the typical characteristic of the matrix structure [29]. GUO et al [30] determined that CaO combined with Fe_2SiO_4 and readily replaced FeO in fayalite, which led to an increase in "free" FeO activity in the slag. Na_2O addition had a similar effect as CaO, i.e., Na^+

ions induced fayalite to release FeO and generated an amorphous sodium−silicon melt. In other words, the [SiO_4] tetrahedral crystal derived from fayalite crystal depolymerization immediately became a matrix state and produced a new broad peak in S4 and S5. The most important absorption peak in this study was indexed to the [SiO_4] tetrahedra symmetric stretching vibration. The broad peak at approximately 800−1200 cm^{-1} linked to the [SiO_4] tetrahedral overlapping bands in Q^n (Q is a Si-centered tetrahedron and n is the number of bridging oxygen atoms [31]) became increasingly distinctive, which reflected the formation of an arsenic-containing matrix in the specimens. To obtain detailed structural information, the broad peak was deconvoluted, and the relative Q^n content characteristics are presented in Fig. 6(b). The relative percentage of (Q^2+Q^3) followed the order of S5, S4, and S6, corresponding to 41.12%, 35.50% and 27.15%, respectively. The Q^2 and Q^3 structures were highly related to the DOP, meaning that the increase in (Q^2+Q^3) content increased the DOP of fayalite. Comparing the (Q^2+Q^3) contents between S5 and S6 illustrated that arsenic significantly enhanced the DOP in the specimen. As^{5+} ions could be incorporated as a glass former ion with fourfold oxygen coordination ([AsO_4]) bonding to [SiO_4] tetrahedral [32], which enhanced the (Q^2+Q^3) content in S5. The FTIR results show that with the increase of sodium arsenate, the fayalite structure depolymerized and released [SiO_4] and [FeO_4] tetrahedra. To further reveal the specific mechanism of the fayalite structure of sodium arsenate depolymerization, we performed XPS analysis on the experimental samples.

Figure 7 shows the XPS results for As 3d and O 1s. The As 3d and O1 s binding energies migrated with increasing arsenate content, which indicated that an arsenic-containing key structure formed in the matrix derived from fayalite. In Fig. 7(a), the As 3d binding energies shifting from 44.63 eV (S2) to 44.95 eV (S5) were strong evidence that the arsenic dissolution species was arsenate. The As 3d binding energy in Na_3AsO_4 was located at approximately 44.29 eV (Fig. 7(b)), which was slightly higher than the value of 43.9 eV in $(AsO_4)^{3-}$ described by KLOPROGGE and WOOD [33]. This kind of binding energy shift is linked to the arsenate chemical environment change. Si, Fe, and Na electronegativity values have been reported as 1.90, 1.83, and 0.93, respectively. For most chemical elements, the higher the electronegativity value of neighboring atoms or the higher the oxidation number/coordination rate of the absorbed atoms in the structural fragments, the greater the shift of the corresponding peaks to higher binding energy values. Therefore, the As 3d peak shift appeared to have been related to higher electronegativities, which

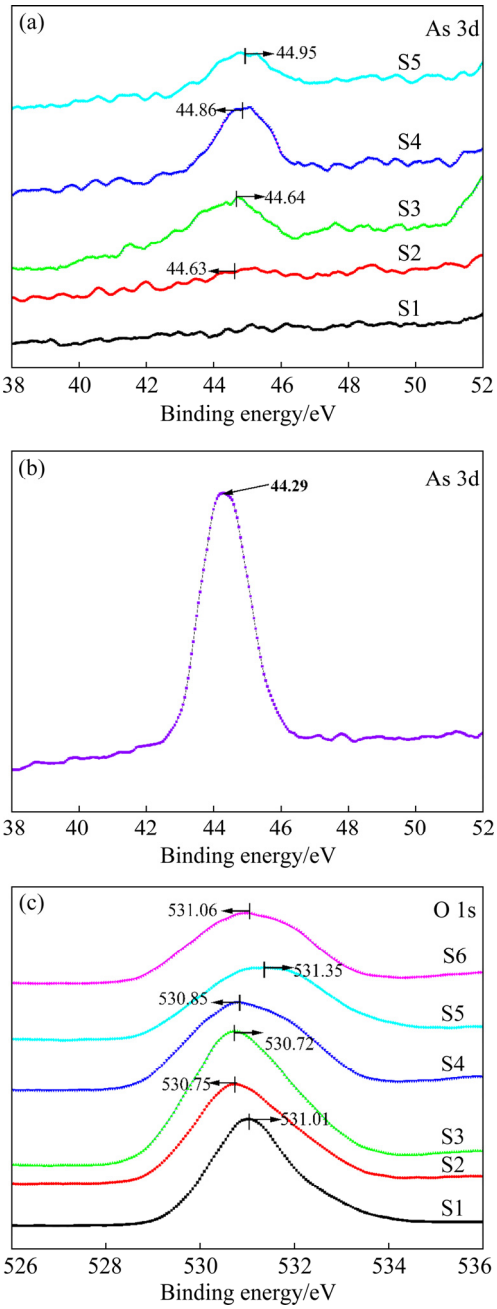

Fig. 7 As 3d spectra of specimens with different initial arsenate additions (a) and Na_3AsO_4 (b), and O 1s spectra of specimens with different initial arsenate additions and with Na_2O (c)

resulted in higher binding energies [34]. In other words, As—O—Si or As—O—Fe substituted As—O—Na during arsenate dissolution in fayalite. The O1 s binding energy showed two different trends due to the depolymerization effect and network-forming effect. When the arsenate content was less than 15 wt.%, the depolymerization effect dominated. The Na^+ ions gradually broke down the fayalite structure and released isolated amorphous [SiO_4] tetrahedra, which resulted in the decreasing binding energy of O1 s in S1−S3. When the arsenate content was over 15 wt.%, the network-forming effect played a leading role in the experiment. The isolated amorphous [SiO_4] tetrahedron bonded with itself or the [AsO_4] tetrahedron by bridging oxygen (BO) and induced Si—O(BO)—As and Si—O(BO)—Si. The BO binding energy was greater than that of nonbridging oxygen (NBO) [35]. Therefore, a comparison between S5 (531.35 eV) and S6 (531.06 eV) indicated a higher BO content in S5 than in S6 due to arsenate dissolution. Specifically, the formation of Si—O(BO)—As bonds caused O1 s to shift to a higher binding energy area.

Figure 8 shows the typical Mossbauer spectra of the specimens. The S1 Mossbauer exhibited a single doublet with an isomer shift (IS) value of 1.15 mm/s, which was due to the two octahedral Fe^{2+} ions in the symmetrical position sites (the fayalite Fe^{2+} ions in the M1 and M2 sites were fitted in S1, and M1 and M2 sites represent the iron sites in Fe—O—Fe and Fe—O—Si respectively) [36]. The fayalite Mossbauer characteristics agreed with our previous study [10]. However, as the arsenate content increased, the two fayalite sub-spectra intensities were weakened. In addition, three other new Fe phases were detected, and the related parameters are shown in Table 3.

The Mossbauer spectrum of S3 was a sum of two sextets with broad lines and two doublets with low peaks. The IS values of the specimens could be used to distinguish Fe phases due to differences in corresponding electron configurations. The IS less than 0.4 mm/s was assigned to tetrahedral Fe^{3+} ions

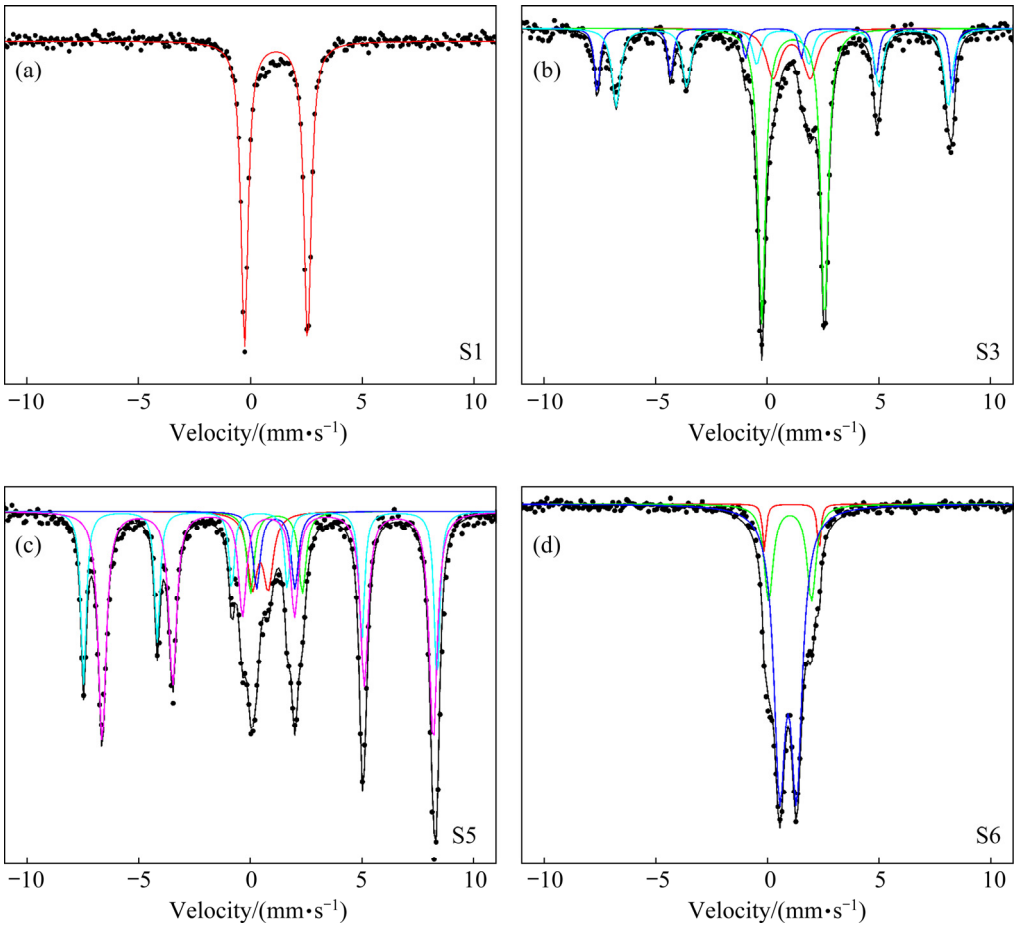

Fig. 8 ^{57}Fe Mossbauer spectra of specimens with different initial arsenate additions: (a) 0% arsenate; (b) 10% arsenate; (c) 20% arsenate; (d) With Na_2O

Table 3 Mossbauer parameters of specimens with different initial arsenate additions

Sample	IS/ ($mm \cdot s^{-1}$)	QS/ ($mm \cdot s^{-1}$)	$\Gamma/2$/ ($mm \cdot s^{-1}$)	Relative area
S1	1.15	2.82	0.19	1
S3	1.09	1.66	0.37	0.133
	1.16	2.8	0.19	0.431
	0.30	-0.07	0.14	0.15
	0.68	0.02	0.22	0.286
S5	0.32	0.68	0.27	0.086
	1.13	1.79	0.26	0.103
	1.16	2.37	0.16	0.052
	0.30	-0.03	0.15	0.258
	0.66	0.03	0.21	0.501
S6	0 .92	0.77	0.31	0.78
	1.00	1.89	0.15	0.129
	1.06	2.45	0.17	0.09

(QS: Quadrupole splitting; $\Gamma/2$: Half-linear width)

and IS was generally more positive for divalent octahedral Fe^{2+} ions [36,37]. Therefore, the two sextets with IS values of 0.3 and 0.68 mm/s were characteristic of Fe^{3+} ions in tetrahedral positions and Fe^{2+} ions in octahedral positions of Fe_3O_4. The hyperfine parameters of the two components were slightly smaller than the values reported in Ref. [38]. The other two doublets with IS values of approximately 1.16 and 1.09 mm/s belonging to Fe^{2+} ions in the fayalite M1 and M2 sites were fitted by least squares, and the S3 Mossbauer results agreed with the XRD results. For the S5 Mossbauer spectrum, Fe_2SiO_4 and Fe_3O_4 were detected. In addition, a new Fe^{3+} phase was detected in S5 with a characteristic IS value of approximately 0.32 mm/s, which was ascribed to the $[FeO_4]$ tetrahedron [35]. Fe_2SiO_4 and FeO were detected in the S6 due to Na^+ ions depolymerizing fayalite Fe — O — Si/Fe — O — Fe. However, no crystal related to Fe^{3+} ions was detected in the XRD measurement, proving that the $[FeO_4]$ tetrahedra were amorphous in S5. In other words, the continued arsenate addition induced matrix generation in the specimen. In addition, the amorphous $[FeO_4]$ tetrahedron formed a network and bonded with the $[SiO_4]$ and $[AsO_4]$ tetrahedrons, building up the matrix network and forming Si—O—As and Fe—O—As bonds [39].

3.4 Fayalite and arsenate TCLP test results

To test the effect of high-temperature reaction on the stability of fayalite and sodium arsenate, the toxicity characteristic leaching procedure (TCLP) test was carried out to the pre-samples (samples S2−S4 before the high-temperature reaction) and the roasted-samples (samples S2−S4 after the high-temperature reaction). The test results are shown in Table 4. It can be seen from Table 4 that as the content of sodium arsenate in the pre-samples increases, the leaching concentration of arsenic also gradually increases, from 1007.61 mg/L of pre-sample S2 to 3025.52 mg/L of pre-sample S5, which indicates that sodium arsenate is highly harmful to the environment. After the high-temperature reaction of sodium arsenate and iron silicate, the arsenic leaching concentration of the roasted samples is significantly lower than the pre-samples, and is controlled below 50 mg/L, which indicates that the high-temperature reaction contributes to the stabilization of sodium arsenate. This is because part of the arsenic volatilized in the form of arsenic element during the high temperature process. On the other hand, the arsenic is fixed in the silicon−oxygen network tetrahedron formed by fayalite, preventing the release of the arsenic. In addition, as the content of sodium arsenate increases, the leaching toxicity of arsenic in roasted samples is on the contrary continuously decreasing. Among them, the leaching toxicity of roasted samples only decreases from 47.54 to 45.89 mg/L while the content of sodium arsenate increases from 10 to 25 wt.%. However, once the addition of sodium arsenate increases to 30 wt.%, the leaching toxicity of arsenic in roasted-sample S5 decreases sharply to 12.8 mg/L. This may be because Na^+ ions, as a network former, can promote the formation of silicon−oxygen tetrahedra and greatly improve the stability of arsenic.

Table 4 Concentrations of arsenic in leachate of samples with different initial arsenate additions after TCLP test (mg/L)

Sample	Before roasting	After roasting
S2	1007.61	47.54
S3	1834.12	46.57
S4	2421.98	45.89
S5	3025.52	12.8

4 Conclusions

(1) With increasing arsenic dosage in raw materials, the mass fraction of arsenic in fayalite-type copper slag increased significantly, but the arsenic distribution proportion decreased in slag.

(2) By studying the phase transition in the reaction process, we found that during the reaction between fayalite and arsenic, the fayalite structure gradually depolymerized and changed from a crystalline state to an amorphous state. Specifically, the isolated crystal [SiO_4] tetrahedron derived from fayalite transformed into an amorphous [SiO_4] tetrahedron.

(3) With increased arsenate content, the fayalite structure depolymerized and released [SiO_4] and [FeO_4] tetrahedra. Subsequently, the [AsO_4] tetrahedron in arsenate combined with the [SiO_4] and [FeO_4] tetrahedra by bridging oxygen to form a glass network structure, which was the key mechanism of arsenic dissolution in fayalite.

(4) After the high-temperature reaction between fayalite and arsenate, residual arsenic is fixed in the silicon−oxygen tetrahedral structure formed by the silicate. This effectively reduces the leaching toxicity of roasted samples.

Acknowledgments

The authors gratefully acknowledge the financial supports from the National Natural Science Foundation of China (No. 51634010), and National Key R&D Program of China (No. 2018YFC1900300).

References

[1] LI Yuan-cheng, MIN Xiao-bo, CHAI Li-yuan, SHI Mei-qing, TANG Cong-jian, WANG Qing-wei, LIANG Yan-jie, LEI Jie, LIYANG Wen-jun. Co-treatment of gypsum sludge and Pb/Zn smelting slag for the solidification of sludge containing arsenic and heavy metals [J]. Journal of Environmental Management, 2016, 181: 756−761.

[2] ALKA S, SHAHIR S, IBRAHIM N, NDEJIKO M J, VO D V N, MANAN F A. Arsenic removal technologies and future trends: A mini review [J]. Journal of Cleaner Production, 2021, 278: 123805.

[3] LIU Wei-feng, FU Xin-xin, YANG Tian-zu, ZHANG Du-chao, CHEN Lin. Oxidation leaching of copper smelting dust by controlling potential [J]. Transactions of Nonferrous Metals Society of China, 2018, 28(9): 1854−1861.

[4] YAO Wen-ming, MIN Xiao-bo, LI Qing-zhu, WANG Qing-wei, LIU Hui, LIANG Yan-jie, LI Kai-zhong, ZHAO Zong-wen, QU Sheng-li, DONG Zhun-qin. Dissociation mechanism of particulate matter containing arsenic and lead in smelting flue gas by pyrite [J]. Journal of Cleaner Production, 2020, 259: 120875.

[5] YU Guo-lin, ZHANG Ying, ZHENG Shi-li, ZOU Xing, WANG Xiao-hui, ZHANG Yi. Extraction of arsenic from arsenic-containing cobalt and nickel slag and preparation of arsenic-bearing compounds [J]. Transactions of Nonferrous Metals Society of China, 2014, 24(6): 1918−1927.

[6] LIU Wei-ping, YIN Xia-fei. Recovery of copper from copper slag using a microbial fuel cell and characterization of its electrogenesis [J]. International Journal of Minerals, Metallurgy, and Materials, 2017, 24: 621−626.

[7] LI Rong, LIN Jin-ru, NILGES M J, CHEN Ning, PAN Yuan-ming. Arsenic speciation in danburite ($CaB_2Si_2O_8$): A synchrotron XAS and single-crystal EPR study [J]. European Journal of Mineralogy, 2014, 26(1): 113−125.

[8] FILATOV S K, KRIVOVICHEV S V, BURNS P C, VERGASOVA L P. Crystal structure of filatovite, $K[(Al,Zn)_2(As,Si)_2O_8]$, the first arsenate of the feldspar group [J]. European Journal of Mineralogy, 2004, 16(3): 537−543.

[9] PAPE P L, BLANCHARD M, BREST J, BOULLIARD J C, IKOGOU M, STETTEN L, WANG Shuai-tao, LANDROT G, MORIN G. Arsenic incorporation in pyrite at ambient temperature at both tetrahedral S−I and octahedral FeII sites: Evidence from EXAFS−DFT analysis [J]. Environmental Science & Technology, 2017, 51(1): 150−158.

[10] WANG Zhong-bing, ZHAO Zong-wen, ZHANG Li-feng, LIU Fan-song, PENG Bing, CHAI Li-yuan, LIU Da-chun, LIU De-gang, WANG Tian-yu, LIU Hui, LIANG Yan-jie. Formation mechanism of zinc-doped fayalite ($Fe_{2-x}Zn_xSiO_4$) slag during copper smelting [J]. Journal of Hazardous Materials, 2019, 364: 488−498.

[11] WANG Zhong-bing, PENG Bing, ZHANG Li-feng, ZHAO Zong-wen, LIU De-gang, PENG Ning, WANG Da-wei, HE Ying-he, LIANG Yan-jie, LIU Hui. Study on formation mechanism of fayalite (Fe_2SiO_4) by solid state reaction in sintering process [J]. JOM, 2018, 70(4): 539−546.

[12] BALLADARES E, KELM U, HELLE S, PARRA R, ARANEDA E. Chemical-mineralogical characterization of copper smelting flue dust [J]. DYNA, 2014, 81(186): 11−18.

[13] MONTENEGRO V, SANO H, FUJISAWA T. Recirculation of Chilean copper smelting dust with high arsenic content to the smelting process [J]. Materials Transactions, 2008, 49(9): 2112−2118.

[14] REDDY R G, FONT J M. Arsenate capacities of copper smelting slags [J]. Metallurgical and Materials Transactions B, 2003, 34(5): 565−571.

[15] ZHAO Zong-wen, SONG Yu-xia, MIN Xiao-bo, LIANG Yan-jie, CHAI Li-yuan, SHI Mei-qing. XPS and FTIR studies of sodium arsenate vitrification by cullet [J]. Journal of Non-Crystalline Solids, 2016, 452: 238−244.

[16] SHI Mei-qing, LIANG Yan-jie, CHAI Li-yuan, MIN Xiao-bo, ZHAO Zong-wen, YANG Shu. Raman and FTIR spectra of modified iron phosphate glasses containing arsenic

[J]. Journal of Molecular Structure, 2015, 1081: 389−394.

[17] HASSAAN M Y, SAUDI H A, SAAD H M H, MOSTAFA A G, AHMED M A, IIDA Y, KUBUKI S, NISHIDA T. Structural study of glass and glass ceramics prepared with Egyptian basalt [J]. Silicon, 2015, 7(4): 383−391.

[18] WANG Qing-meng, GUO Xue-yi, TIAN Qing-hua, CHEN Mao, ZHAO Bao-jun. Reaction mechanism and distribution behavior of arsenic in the bottom blown copper smelting process [J]. Metals, 2017, 7(8): 302.

[19] WANG Qing-meng, GUO Xue-yi, TIAN Qing-hua, CHEN Mao, ZHAO Bao-jun. Effects of matte grade on the distribution of minor elements (Pb, Zn, As, Sb, and Bi) in the bottom blown copper smelting process [J]. Metals, 2017, 7(11): 502.

[20] ZHAO Zong-wen, CHAI Li-yuan, LIANG Yan-jie, MIN Xiao-bo, FEI Jiang-chi, MA Jing-jing. The vitrification of arsenic-rich residue using iron phosphate glass [J]. Physics and Chemistry of Glasses-European Journal of Glass Science and Technology Part B, 2017, 58(6): 109−114.

[21] ROUQUETTE J, KANTOR I, MCCAMMON C A, DMITRIEV V, DUBROVINSKY L S. High-pressure studies of $(Mg_{0.9}Fe_{0.1})_2SiO_4$ olivine using Raman spectroscopy, X-ray diffraction, and Mössbauer spectroscopy [J]. Inorganic Chemistry, 2008, 47(7): 2668−2673.

[22] BASITH N M, VIJAYA J J, KENNEDY L J, BOUOUDINA M, SHENBHAGARAMAN R, JAYAVEL R. Influence of Fe-doping on the structural, morphological, optical, magnetic and antibacterial effect of ZnO nanostructures [J]. Journal of Nanoscience and Nanotechnology, 2016, 16(2): 1567−1577.

[23] FEYGENSON M, BAUER J C, ZHENG Gai, MARQUES C; ARONSON M C, TENG Xiao-fei, SU Dong, STANIC V, URBAN V S, BEYER K A, DAI Sheng. Exchange bias effect in Au-Fe_3O_4 dumbbell nanoparticles induced by the charge transfer from gold [J]. Physical Review B: Condensed Matter, 2015, 92(5): 054416−054429.

[24] SONG Fei, YU Zheng-lei, YANG Feng-ling, LU Yi-nong, LIU Yun-fei. Microstructure of amorphous aluminum hydroxide in belite-calcium sufflaminate cement [J]. Cement and Concrete Research, 2015, 71: 1−6.

[25] MARANGONI M, ARNOUT L, MACHIELS L, PANDELAERS L, BERNARDO E, COLOMBO P, PONTIKES Y. Porous, sintered glass-ceramics from inorganic polymers based on fayalite slag [J]. Journal of the American Ceramic Society, 2016, 99(6): 1985−1991.

[26] QAFOKU O, ILTON E S, BOWDEN M E, KOVARIK L, ZHANG Xin, KUKKADAPU R K, ENGELHARD M H, THOMPSON C J, SCHAEF H T, MCGRAIL B P, ROSSO K M, LORING J S. Synthesis of nanometer-sized fayalite and magnesium-iron(II) mixture olivines [J]. Journal of Colloid and Interface Science, 2018, 515: 129−138.

[27] MACDONALD S A, SCHARDT C R, MASIELLO D J, SIMMONS J H. Dispersion analysis of FTIR reflection measurements in silicate glasses [J]. Journal of Non-Crystalline Solids, 2000, 275(1/2): 72−82.

[28] HOFMEISTER A M. Single-crystal absorption and reflection infrared spectroscopy of forsterite and fayalite [J]. Physics and Chemistry of Minerals, 1987, 14(6): 499−513.

[29] NAYAK M T, DESA J A, BABU P D. Magnetic and spectroscopic studies of an iron lithium calcium silicate glass and ceramic [J]. Journal of Non-Crystalline Solids, 2018, 484: 1−7.

[30] GUO Zheng-qi, ZHU De-gang, PAN Jan, ZHANG Feng. Mechanism of mineral phase reconstruction for improving the beneficiation of copper and iron from copper slag [J]. JOM, 2016, 68(9): 2341−2348.

[31] BANCROFT G M, NESBITT H W, HENDERSON G S, O'SHAUGHNESSY C, WITHERS A C, NEUVILLE D R. Lorentzian dominated lineshapes and linewidths for Raman symmetric stretch peaks (800−1200 cm^{-1}) in Q^n ($n = 1−3$) species of alkali silicate glasses/melts [J]. Journal of Non-Crystalline Solids, 2018, 484: 72−83.

[32] PAJE S E, GARCIA M A, LLOPIS J, VILLEGAS M A. Optical spectroscopy of silver ion-exchanged as-doped glass [J]. Journal of Non-Crystalline Solids, 2003, 318(3): 239−247.

[33] KLOPROGGE J T, WOOD B J. X-ray photoelectron spectroscopic and Raman spectroscopic study of bayldonite from Wheal Carpenter, Cornwall, UK [J]. Vacuum, 2017, 141: 49−56.

[34] GOLOVCHAK R, SHPOTYUK Y, THOMAS C M, NAZABAL V, PLEDEL C B, BUREAU B, JAIN H. Peculiarities of Ga and Te incorporation in glassy arsenic selenides [J]. Journal of Non-Crystalline Solids, 2015, 429: 104−111.

[35] ZHAO Zong-wen, CHAI Li-yuan, PENG Bing, LIANG Yan-jie, HE Ying-he, YAN Zhi-hao. Arsenic vitrification by copper slag based glass: Mechanism and stability studies [J]. Journal of Non-Crystalline Solids, 2017, 466/467: 21−28.

[36] HASSAAN M Y, MOUSTAFA M G, OSOUDA K, KUBUKI S, NISHIDA T. 57Fe and 119Sn Mössbauer, XRD, FTIR and DC conductivity study of $Li_2OFe_2O_3SnO_2P_2O_5$ glass and glass ceramics [J]. Journal of Alloys and Compounds, 2018, 765: 121−127.

[37] KUCZEK J, JELEN P, STOCH P, BLACHOWSKI A, WACLAWSKA I, SZUMERA M. Raman and Mossbauer studies of iron phosphate-silicate glasses [J]. Journal of Molecular Structure, 2018, 1170: 82−89.

[38] MIR L E, GHOUL J E, ALAYA S, SALEM M B, BARTHOU C, BARDELEBEN H J. Synthesis and luminescence properties of vanadium-doped nanosized zinc oxide aerogel [J]. Physica B: Condensed Matter, 2008, 403(10/11): 1770−1774.

[39] TAKEBE H, TOMITA S, SAITOH A, KAWAHARA M, SUEOKA Y, SAKAKIBARA M. Effect of crystallization on microstructure and elution properties in copper slag [J]. Journal of Sustainable Metallurgy, 2017, 3(3): 543−550.

高温过程中砷酸盐与铁橄榄石型铜渣的反应机制

王大伟[1]，赵宗文[1]，林 璋[1,2]，梁彦杰[1,2]，康 丽[1]，彭 兵[1]

1. 中南大学 冶金与环境学院，长沙 410083；
2. 国家重金属污染防治工程技术研究中心，长沙 410083

摘 要：通过 XRD、XPS、HRTEM 和 TCLP 等技术手段和方法研究砷酸钠与铁橄榄石在 1200 °C 下的反应机制。结果表明，砷酸钠进入到渣相与气相中的比例分别约为 30%和 70%。砷酸钠的添加使铁橄榄石结构解聚，并将其从结晶态转变为非结晶态。铁橄榄石结构变化表明，砷酸钠中的[AsO_4]四面体与[SiO_4]四面体和[FeO_4]四面体通过桥氧键结合形成硅酸盐玻璃结构。铁橄榄石与砷酸钠高温反应前后样品的 TCLP 测试结果表明，高温反应能显著降低砷酸钠的浸出毒性，样品中砷的浸出浓度由反应前的 3025.52 mg/L 降低到反应后的 12.8 mg/L。

关键词：铁橄榄石；砷酸钠；聚合反应；硅酸盐玻璃结构

(Edited by Xiang-qun LI)